Threshold Meson Production in Proton–Proton Interactions at the Internal Beam Facility COSY–11

November 5, 1999

M. Wolke[1], H.-H. Adam[2], J.T. Balewski[1,3,4], A. Budzanowski[3], C. Goodman[4], D. Grzonka[1], L. Jarczyk[5], M. Jochmann[6], A. Khoukaz[2], K. Kilian[1], M. Köhler[6], P. Kowina[7], N. Lang[2], T. Lister[2], P. Moskal[1,5], W. Oelert[1], C. Quentmeier[2], R. Santo[2], G. Schepers[1,2], U. Seddik[8], T. Sefzick[1], S. Sewerin[1], M. Siemaszko[7], J. Smyrski[5], M. Sokolowski[5], A. Strzałkowski[5], P. Wüstner[6], W. Zipper[7]

(1) Institut für Kernphysik, Forschungszentrum Jülich, D–52425 Jülich, Germany

(2) Institut für Kernphysik, Westfälische Wilhelms–Universität, D–48149 Münster, Germany

(3) Institute of Nuclear Physics, PL–31–342 Cracow, Poland

(4) Indiana University Cyclotron Facility, Bloomington, IN 47405, USA

(5) Institute of Physics, Jagellonian University, PL–30–059 Cracow, Poland

(6) Zentrallabor für Elektronik, Forschungszentrum Jülich, D–52425 Jülich, Germany

(7) Institute of Physics, University of Silesia, PL–40–007 Katowice, Poland

(8) Egyptian Atomic Energy Authority, 13759 Cairo, Egypt

Introduction

At medium energy proton storage rings with phase space cooling, IUCF in Bloomington, CELSIUS in Uppsala and COSY in Jülich, the production of mesons near threshold has been subject of detailed studies during the last years. Experimental data obtained at complementary facilities provide access to both the underlying reaction mechanisms and the structure of mesons and baryons.

The COoler SYnchrotron at the Forschungszentrum Jülich delivers a phase space cooled beam with proton energies up to 2.6 GeV using both electron and stochastic cooling. At present, beam intensities of 4×10^{10} stored protons are provided. The high quality beam with a relative momentum resolution $\Delta\, p/p \leq 10^{-4}$ and emittances $\varepsilon \leq 1\,\pi\,\mathrm{mm\,mrad}$ serves internal and external experiments. Portraits of the accelerator and experimental facilities are given in more detail in [1].

The COSY–11 installation is an internal facility at COSY designed for threshold meson production studies. Close to threshold only few partial waves contribute to the scattering amplitudes, which simplifies the theoretical interpretation. Due to low relative velocities of the ejectiles and, consequently, extended interaction times, effects of low energy baryon–baryon, meson–baryon and meson–meson final state interaction have a strong effect on the measured observables. At the same time, a large momentum transfer probes the short range part of the nucleon–nucleon force.

Experimentally, due to small transverse momenta, close to threshold all ejectiles are limited to a narrow forward cone in the laboratory system. A high geometrical acceptance is attainable with a comparatively small detector setup.

The COSY–11 Facility

In spring 1995 the COSY–11 facility [2] has been installed at an internal target location in a bending section of the cooler synchrotron (figs. 1,2).

A cluster target [3] is located in front of a normal C–shaped COSY dipole. When passing a Laval type nozzle a pre–cooled gas condensates under appropriate conditions and clusters of up to 10^6 molecules grow. As clusters are heavy compared with residual gas molecules, the influence of collisions on the divergence of the cluster beam is negligible. Instead, the spread of the beam is defined geometrically by skimmer and collimator apertures. Decoupling the nozzle region by differential pumping stages, which are passed by the cluster beam, UHV conditions are maintained in the scattering chamber. Densities of about $10^{14}\,\mathrm{atoms/cm^3}$ are reached routinely in case of a hydrogen target with a diameter of $\approx 9\,\mathrm{mm}$. Deuteron cluster beams have been produced with comparable densities, and the mechanism is also applicable to other gases.

Charged reaction products are separated by the magnetic field from the circulating beam due to their lower momenta. A specially designed chamber with large exit windows replaces the standard dipole vacuum chamber: The exit window ($187 \times 7.6\,\mathrm{cm^2}$) for positively charged reaction products is covered by a sandwich arrangement composed of a $30\,\mu$m aluminium layer and two sheets of $150\,\mu$m carbon fibres. Thus, straggling caused by this foil is limited

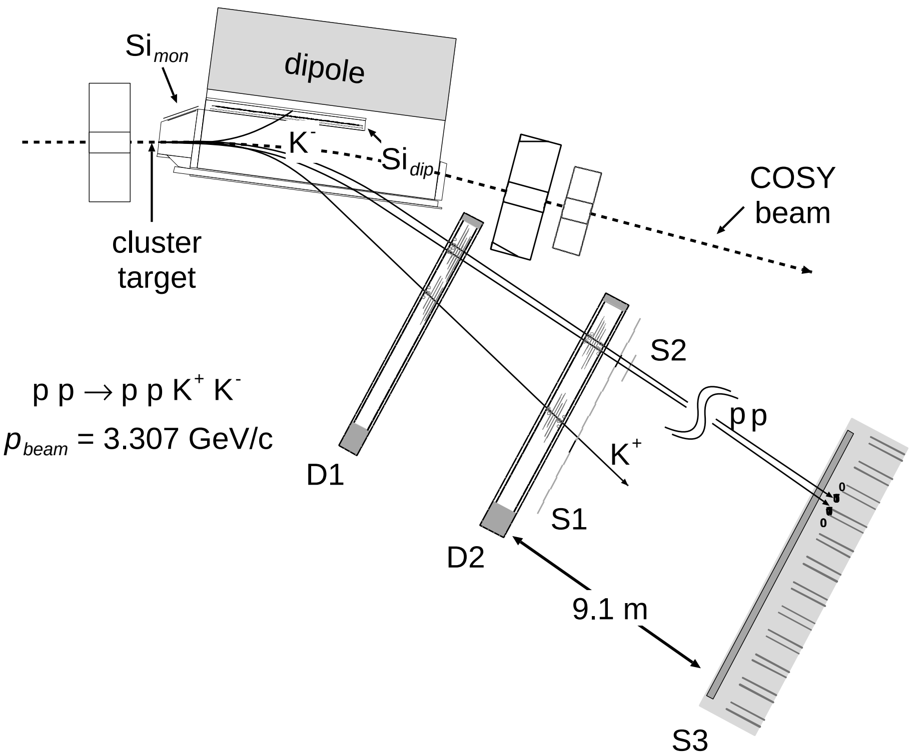

Figure 1: Schematic view of the internal COSY–11 installation.

to values below the resolution of the detection system.

A momentum analysis for positively charged ejectiles is achieved from the deflection in the dipole field, measured using two sets of drift chamber stacks (marked D1, D2 in fig. 1), each set consisting of planes with vertical and inclined wires. The 40 mm wide drift cells are of the graded–field type and position resolutions of 200 μm are achieved in each plane. Particle momenta are reconstructed via ray tracing back of the trajectories through the well–known dipole field to the target position.

Two scintillator hodoscopes (S1 and S2 in fig. 1) determine at the trigger level the multiplicity of charged tracks in the exit channel. Close to threshold protons from the pp $\to$ ppX reaction, where X denotes an uncharged meson or mesonic system, are confined to a narrow cone, which is covered by the S2 scintillator up to several MeV excess energy in the final state (fig. 1). Thus, close tracks hitting the same 10 cm wide segment of the S1 scintillator are resolved by the higher granularity (1.3 cm) of the movable S2 arrangement. Even closer tracks are recognized via signal amplitude.

The S1/S2 scintillator hodoscopes provide the start signal for a time–of–flight measurement used for particle identification. The stop signal is generated by the large area scintillation wall S3 [2,4] placed 9.1 m downstream. The $2.2 \times 1\,\mathrm{m}^2$ large scintillator plate is viewed by a matrix arrangement of 217 photomultipliers.

A particle identification is achieved from the combination of momentum reconstruction

Figure 2: The COSY–11 facility in the target region. Pumping stages of the cluster target are seen in the upper part of the photograph, followed by the momentum analyzing dipole. Positively charged reaction products are detected in two drift chamber stacks and a scintillator hodoscope arrangement depicted in the lower part of the figure.

and time–of–flight information via the invariant mass

$$m_{inv}^2 = \frac{|\vec{p}\,|^2}{\beta^2\gamma^2}, \tag{1}$$

where $\vec{p}$ denotes the particle momentum, β its velocity in units of the light velocity and $\gamma = 1/\sqrt{1-\beta^2}$. With momentum vector and particle mass the complete four–momentum vector $(E^f, \vec{p}^{\,f})$ of the outgoing charged particle is determined.

Negatively charged mesons, with their tracks being bent towards the yoke of the dipole, are detected by a scintillation counter and an array of silicon pad detectors (Si_{dip}) with a granularity of 5 mm horizontally and 20 mm vertically, both mounted inside the dipole gap.

Neutral mesons or baryons are not detected directly, instead, they are identified using the missing mass method: ¿From the known four–momenta of both the target nucleus and the projectile $(E^i, \vec{p}_{beam})$ and the measured four–momenta of positively charged ejectiles $(E^f_j, \vec{p}^{\,f}_j)$ the missing mass with respect to n identified particles in the final state is evaluated as the four–momentum balance of the subsystem:

$$\mathcal{M}^2_n = \left(E^i - \sum_{j=1}^{n} E^f_j\right)^2 - \left(\vec{p}_{beam} - \sum_{j=1}^{n} \vec{p}^{\,f}_j\right)^2 \qquad (2)$$

with the total energy in the initial state $E^i = \sqrt{m_p^2 + \vec{p}^{\,2}_{beam}} + m_p$. In case of a three particle final state pp $\rightarrow$ 1 2 3 the missing mass with respect to the subsystem (1 2) is of course equal to the mass of particle 3.

Figure 3 gives an impression of the performance of the COSY–11 detection system: On the scale of the invariant mass (eq. 1) different charged ejectiles as pions, kaons and protons are cleanly separated, the missing mass technique (eq. 2) allows the identification of different reaction channels.

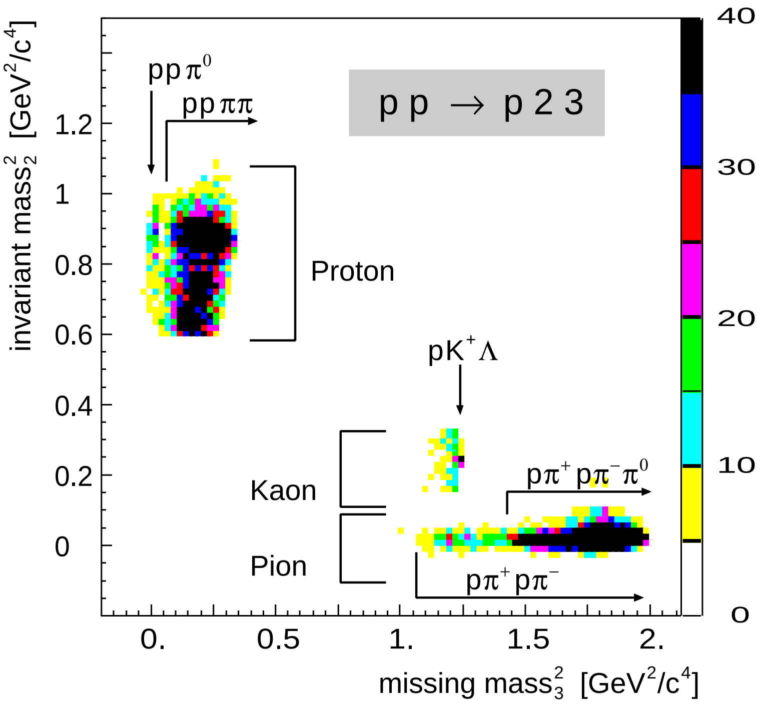

Figure 3: Event identification at the COSY–11 facility for reactions pp $\rightarrow$ p 2 3 from a measurement slightly above the p$K^+\Lambda$ threshold. The invariant mass of a second charged particle in addition to an identified proton is plotted versus the missing mass with respect to the (p 2) subsystem, i.e. versus the mass of the third undetected particle or particle system.

For an absolute normalization of the observed counting rates, events from proton–proton elastic scattering are recorded simultaneously during each measurement. The additional silicon pad detector Si_{mon} is used to measure elastically scattered protons in coincidence with the forward part of the detection system, i.e. drift chambers and S1 hodoscope. Elastic cross section data of high precision for the whole COSY energy range are available from measurements by the EDDA collaboration [5] at COSY. Typical luminosities at COSY–11 are in the order of $4 \times 10^{30}\,\mathrm{cm}^{-2}\mathrm{s}^{-1}$.

Both geometrical coverage and detection efficiencies of the COSY–11 facility are considered to determine the overall acceptance using Monte Carlo simulations of the detection system. In order to derive absolute cross section values, measured counting rates are related to the experimental value of the luminosity and the Monte Carlo based acceptance study.

The large area exit window of the dipole chamber provides high acceptance compared to conventional magnetic spectrometers. Figure 4 depicts the area of acceptance in terms of transversal and longitudinal momenta in units of the beam momentum. In the vertical direction, the opening of the dipole gap with an internal height of 60 mm limits the integral acceptance of the COSY–11 facility. Therefore a full geometrical acceptance at threshold drops down to a typical level of $\approx$ 25 % at excess energies of 10 MeV for the two proton detection in reactions of the type pp $\to$ ppX. However, even at higher excess energies the full range of relevant polar scattering angles is covered.

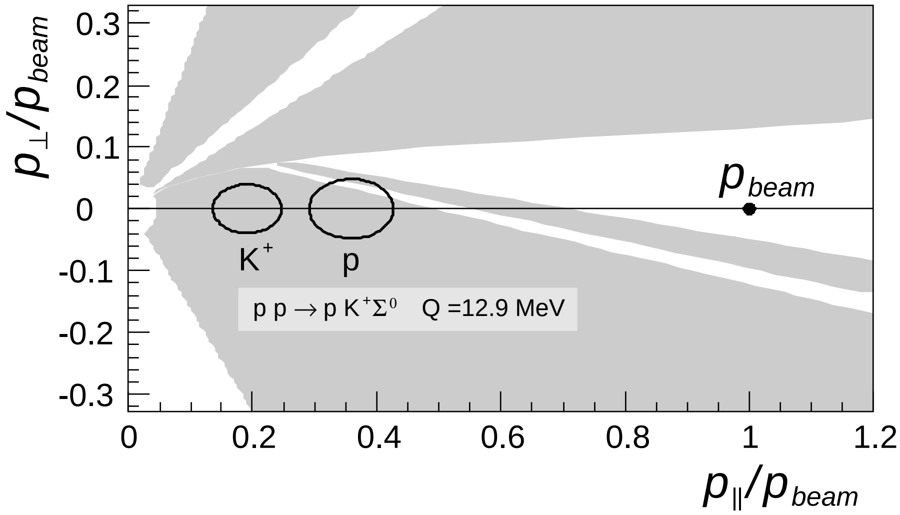

Figure 4: Geometrical acceptance of the COSY–11 facility for positively charged particles as a function of transversal ($p_\perp$) and longitudinal ($p_{||}$) momentum components in units of the beam momentum. Momentum ratios within the shaded regions are detected. In comparison, kinematically allowed momentum ranges for protons and positively charged kaons are indicated for the reaction pp $\to$ p$K^+\Sigma^0$ at an excess energy of 12.9 MeV.

Consequently, the design of the experimental installation focusses on threshold studies, implementing a 4π internal magnetic spectrometer directly at threshold.

Experimental Programme

Since data taking at COSY–11 started in April 1995, the threshold production of strange and non–strange mesons in proton–proton scattering is being investigated. The physics programme covers the production of uncharged isoscalar (η, η') and vector (ω, Φ) mesons, of charged meson pairs without and with strangeness in the $\pi^+\pi^-$ and the K^+K^- systems, respectively, as well as the hyperon production channels $pp \to pK^+\Lambda/\Sigma^0$. Very recently, the experimental programme has been extended to η and η' production in the reactions $pd \to {}^3HeX$ using a deuterium cluster target.

Results on η' production in proton–proton scattering and hyperon production via $pp \to pK^+Y$ are discussed as examples for the experimental technique, the capabilities of the internal facility and physics implications from threshold experiments at COSY–11.

Threshold η'(958) Production

Within the SU(3)–flavour meson nonets, i.e. the classification of $q\bar{q}$ combinations according to their total spin J, parity P and C–parity quantum numbers, states with identical additive quantum numbers — isospin I and strangeness S — are allowed to mix. In the pseudoscalar sector ($J^{PC} = 0^{-+}$, fig. 5) the experimentally observable mesons η and η' can be described as linear combinations of the isospin $I = 0$ octet state η_8 and the pseudoscalar singlet η_1, characterized by a mixing angle Θ_{PS}. With an experimental value of $\Theta_{PS} = -15.5°$ the strangeness contents in both wavefunctions are about equal, thus, similar masses are expected.

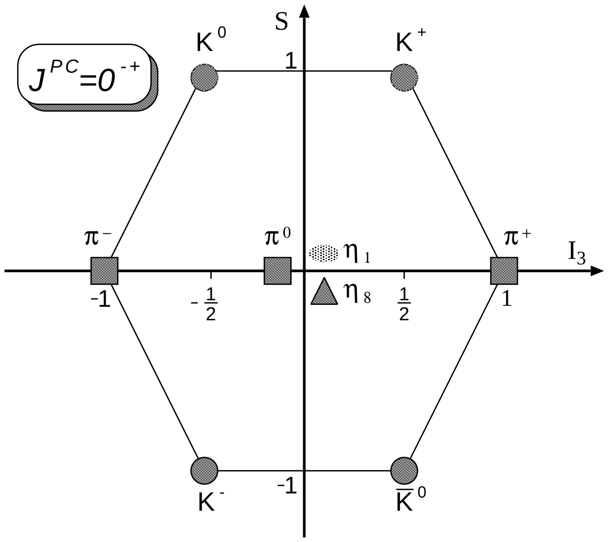

$$\eta_8 = \frac{1}{\sqrt{6}}\,(u\bar{u} + d\bar{d} - 2s\bar{s}) \qquad \eta = \cos\Theta_{PS}\,\eta_8 - \sin\Theta_{PS}\,\eta_1$$

$$\eta_1 = \frac{1}{\sqrt{2}}\,(u\bar{u} + d\bar{d} + s\bar{s}) \qquad \eta' = \sin\Theta_{PS}\,\eta_8 + \cos\Theta_{PS}\,\eta_1$$

Figure 5: The SU(3)–flavour pseudoscalar meson nonet. The strangeness quantum number S is plotted versus the third component I_3 of the isospin. Experimentally observable states η and η' are mixtures of the $I = 0$ octet member η_8 and the singlet state η_1, Θ_{PS} denotes the mixing angle.

The observation that the η'(958) has almost twice the mass of the η(547) has led to speculations about significant admixtures in the wavefunction in addition to a pure non–

strange and strange quark content. A possible contribution are two gluon states coupling to the flavour singlet state, i.e. predominantly the η', and these might account for the η' mass [6].

At the COSY–11 installation, the reaction pp $\to$ ppη' has been studied close to threshold [7]. A typical missing mass spectrum with respect to an identified (pp) subsystem is shown in figure 6. With a stochastically cooled beam a missing mass resolution for the η' of 0.7 MeV/c^2 is achieved at an excess energy, i.e. total centre–of–mass kinetic energy in the final state, of 7.6 MeV. The smooth background structure, which is determined from a measurement below the η' threshold, results from multi–pion production. Obviously, a high missing mass resolution is essential to achieve a reasonable signal–to–background ratio. After correcting for the respective kinematical limit and different integrated luminosities, the background is subtracted and total cross sections are derived from the resulting counting rates.

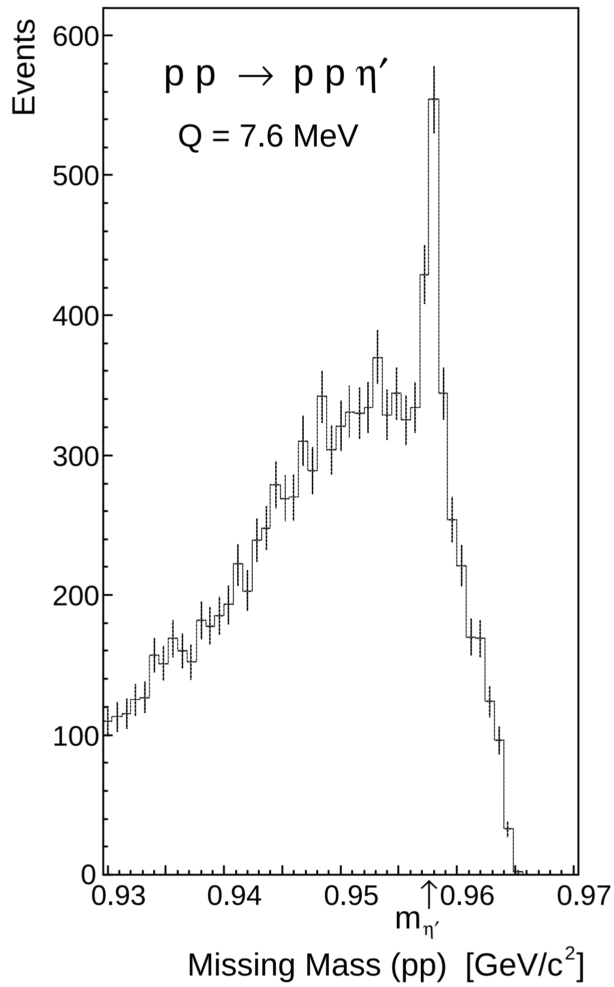

Figure 6: Missing mass of the identified (pp) system measured at an excess energy of 7.6 MeV with respect to the η' threshold. The smooth background is explained by the production of two or three pions. In the range of the η' a missing mass resolution of 0.7 MeV/c^2 is achieved.

Total cross sections for close to threshold η' production in proton–proton scattering measured at COSY–11 are shown in figure 7 in comparison with results for π^0, η, and η' production [8] from IUCF, CELSIUS and SATURNE. As a function of the maximum meson momentum in the centre–of–mass system in units of the produced meson mass, π^0 and η' production in proton–proton scattering occur at the same scale, whereas η production shows a much higher reaction probability (fig. 7b). A large η production amplitude can be explained by a dominant production amplitude via the S_{11} nucleon resonance $N^*(1535)$ coupling to the $N\eta$ channel (with N denoting a nucleon). With only low partial waves involved, possible resonances do not contribute close to threshold in case of π^0 or η' production. It should be noted, however, that at equal excess energies the π^0 cross sections exceed the η' production by about a factor of 50, which happens to correspond to the mass ratio squared (fig. 7a).

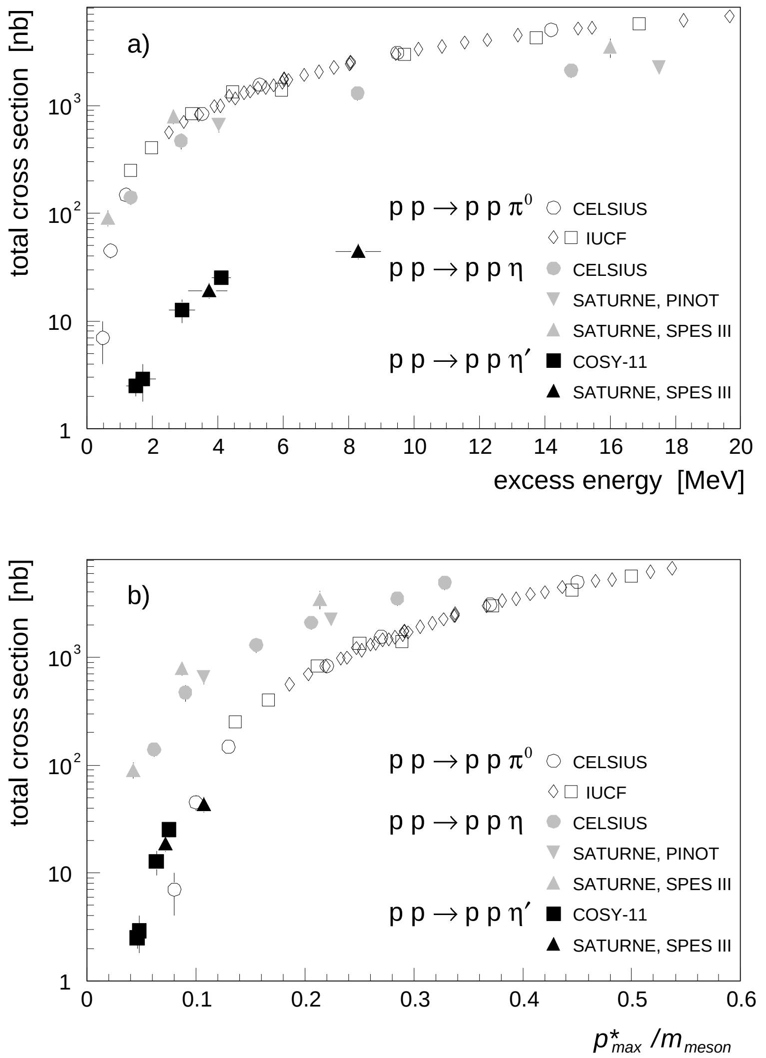

Figure 7: Total cross sections of the reactions $pp \to pp\pi^0$, $pp \to pp\eta$, and $pp \to pp\eta'$ close to threshold as a function of the excess energy (a) and the maximum meson momentum in the centre–of–mass system in units of the meson mass (b). Data are taken from [7, 8].

With high momentum transfers between the scattered protons, the η' production is expected to be sensitive to the short range part of the nucleon–nucleon interaction. More speculative, a two gluon fusion has been suggested as a short range contribution to the η' production amplitude [9] and threshold production data might probe the gluonic content of the η' wave function.

Additional data for the η' production have been taken at the COSY–11 facility up to excess energies of 24 MeV and preliminary results have already been presented [10]. The η and η' physics programme is intended to be continued with high statistics Dalitz plot type of studies.

Associated Strangeness Production via $pp \to pK^+\Lambda/\Sigma^0$

At COSY energies, in proton–proton collisions the associated strangeness production is accessible via the dissociation of the strange–antistrange quark pair into a kaon–hyperon system (e.g. $pp \to pK^+\Lambda$), a kaon–antikaon system (e.g. $pp \to ppK^+K^-$), or via the creation of a single strange–antistrange meson ($pp \to pp\Phi$).

The production cross sections of the isoscalar Λ and the isovector Σ^0 hyperon in the proton–proton interaction have been studied in the $pp \to pK^+Y$ reaction [11, 12]. Again, the hyperon is identified using the missing mass technique from the kinematically complete four–momentum information for the (pK^+) system.

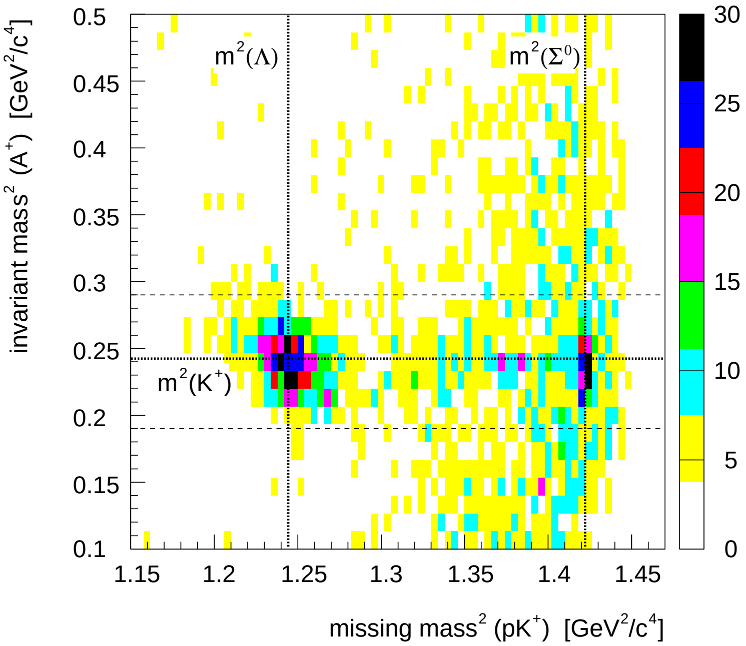

Figure 8: Invariant mass squared of a second charged particle in addition to an identified proton versus the missing mass squared of the assumed (pK^+) subsystem at an excess energy of 12.9 MeV with respect to the Σ^0 threshold. The range of identified kaons is limited by a cut equivalent to three standard deviations of the K^+ invariant mass distribution.

The invariant mass squared of a second charged particle in addition to an identified proton in the exit channel is shown as a function of the missing mass squared of the assumed (pK^+) subsystem in figure 8 for a measurement at an excess energy Q = 12.9 MeV with respect to the Σ^0 production threshold. Kaons are clearly observed within the experimental resolution on the invariant mass scale with enhancements of the (pK^+) missing mass at the Λ and Σ^0 mass, respectively. The projection onto the missing mass scale for events with an identified (pK^+) subsystem is presented in figure 9a. The background is determined from equivalent projections of the adjacent bands outside the region of identified kaons indicated in figure 8. The missing mass spectrum after background subtraction is shown in figure 9b. The width of the Λ peak — when compared to the peak in the Σ^0 mass region — is a kinematic effect, as the missing mass resolution scales with the square root of the excess energy.

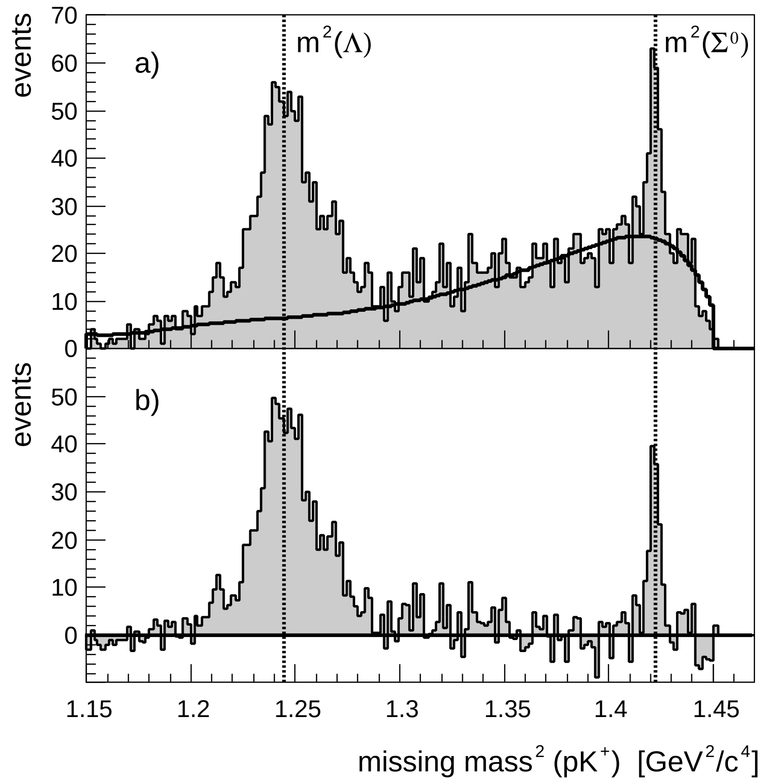

Figure 9: Missing mass squared with respect to the (pK^+) subsystem at an excess energy of 12.9 MeV above the Σ^0 threshold. The spectrum is obtained by projecting events with an additional identified kaon (fig. 8) onto the missing mass axis (a). The background (solid line) is derived from the projection of adjacent bands, resulting counting rates after background subtraction are shown in (b).

In general, the total production cross section is proportional to the square of the transition matrix element M integrated over the available phase space. The transition matrix element contains both the dynamics of the reaction and the low energy elastic interaction of the outgoing particles in the final state. Assuming the basic production mechanisms to be constant at small energy changes, the final state interaction (FSI) varies due to the changes in the kinetic energy of the final state system. According to the Watson approximation [13], the FSI can be factored out from the transition matrix element as

$$\begin{aligned}\sigma_{tot} &\propto \int |M|^2 d\rho \\ &\approx |M_0|^2 \int |M_{FSI}|^2 d\rho \end{aligned} \quad (3)$$

where the constant M_0 contains the dynamical information and determines the scale of the cross section. The energy dependence is given essentially by the phase space volume modified by the final state interaction. For a three particle final state, the available phase space scales with the square of the excess energy.

Due to a rapidly changing cross section at threshold, a precise knowledge of the excess energy is indispensable for the interpretation of data. Considering only small steps in energy, the beam optics of the cooler synchrotron remain essentially unchanged and the relative error is determined by the accuracy of the revolution frequency. This is known to much higher precision than the orbit length for a given beam optics. The latter limits the knowledge on the actual beam momentum to $\Delta p/p \approx 10^{-3}$, corresponding to an uncertainty of ≈ 0.9 MeV in excess energy at the hyperon thresholds. The observed counting rate in case of the $pp \rightarrow pK^+\Lambda$ reaction, normalized to the integrated luminosity, is shown as a function of the excess energy in figure 10.

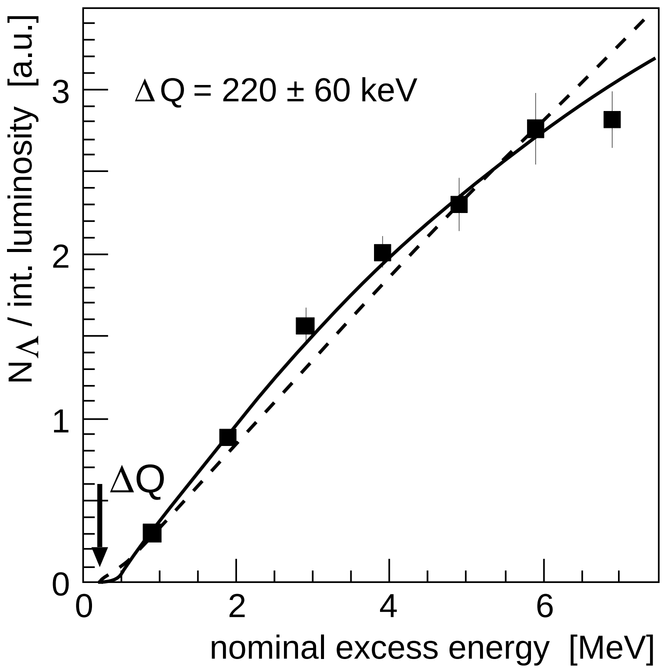

Figure 10: Determination of the true excess energy from the experimentally observed counting rate for the reaction $pp \rightarrow pK^+\Lambda$ close to threshold. The energy dependence is described by a phase space behaviour modified by final state interaction effects (solid line). In comparison, the pure phase space calculation is included (dashed line). The arrow marks a resulting shift in excess energy of 220 ± 60 keV with respect to the nominal value.

Obviously, the energy dependence is much better reproduced by a phase space behaviour modified by the dominant (pΛ) FSI and the Coulomb interaction in the (pK^+) subsystem than by a pure phase space description both normalized to the data. The extrapolation of the counting rate to zero determines the true excess energy with a precision of 60 keV, i.e. one order of magnitude below the uncertainty from machine parameters.

Total cross sections for Λ and Σ^0 production up to excess energies of Q = 12.9 MeV are shown in figure 11. At equal excess energies, the Λ production is strongly favoured over the Σ^0 production with

$$\frac{\sigma_T\left(\mathrm{pp}\to\mathrm{pK}^+\Lambda\right)}{\sigma_T\left(\mathrm{pp}\to\mathrm{pK}^+\Sigma^0\right)} \approx 28\,^{+9}_{-6} \tag{4}$$

in the energy range considered here, whereas at excess energies > 300 MeV the ratio is known to be ≈ 2.5 [15].

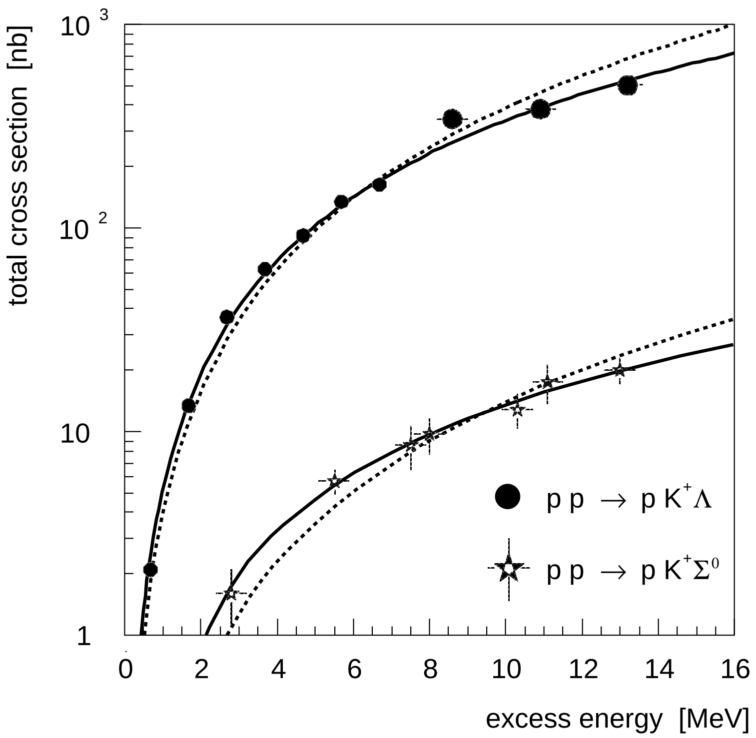

Figure 11: Data on the total cross section for the reactions pp $\to$ p$K^+\Lambda$ and pp $\to$ p$K^+\Sigma^0$ obtained at COSY–11 [11, 12]. The statistical error is included or is smaller than the symbol size. Horizontal error bars denote the uncertainty of the true excess energy. The energy dependence is much better described by a phase space behaviour modified by the proton–hyperon final state interaction (solid line [14]) than by a pure phase space calculation (dashed line).

Qualitative arguments indicate a strong ΣN $\to$ Λp final state conversion to account for the depletion of the Σ^0 signal in the COSY–11 data [12]. On the other hand, first theoretical results obtained within the framework of the Jülich meson exchange model, describing the production mechanism in terms of the relevant degrees of freedom, conclude Λ production to be dominated by kaon exchange while both kaon and pion exchange are expected to contribute with similar strength to Σ^0 production. As a result, the Σ^0 suppression can be explained by a destructive interference of kaon and pion exchange [16]. However, direct production, the exchange of heavier mesons $(\rho, \omega, \mathrm{K}^*)$ and the influence of nucleon resonances [16–18] might be important.

Future COSY–11 measurements at higher excess energies will determine the energy dependence of the observed Σ^0 depletion. Tests in differently charged final states, for example $\mathrm{pp} \to \mathrm{nK}^+\Sigma^+$, will probe the Λ/Σ production ratio in complementary isospin configurations and will thus contribute additional constraints on theoretical interpretations.

From Present to Future

Threshold experiments will be continued at COSY–11 both in proton–proton and proton–deuteron scattering.

In addition to hyperon and η' studies data on the proton–proton induced threshold production of η, ω, Φ and $\mathrm{K}^+\mathrm{K}^-$ are presently analyzed. In case of the elementary kaon–antikaon production channel, despite low cross sections in the vicinity of broad hyperon resonances, the four particle final state is identified exclusively. Sufficiently high luminosities will allow the determination of the excitation function close to threshold for $\mathrm{K}^+\mathrm{K}^-$ production in future.

The development of a polarized beam at COSY provides new tools to disentangle different production mechanisms: Non–isotropic differential cross sections for η production at excess energies below 40 MeV suggest an influence of higher partial waves [19]. Experimentally, the η analyzing power, i.e. the normalized difference of spin dependent differential cross sections, is sensitive to the d–wave amplitude and, at the same time, should probe a possible p–wave influence from different angular distributions. A first beam time to study η production with a polarized beam is scheduled at COSY–11 for early 2000.

The COSY–11 facility has proven to be a powerful tool for threshold studies. The collaboration will continue the dedicated experimental programme at a facility, which is at the same time open to new ideas in experimental medium energy physics.

References

[1] R. Maier, *Nucl. Phys. News Int.* **7** (1997) No. 4, 5 and R. Maier, *Nucl. Instr. & Meth.* **A 390** (1997) 1.

[2] S. Brauksiepe et al., *Nucl. Instr. & Meth.* **A 376** (1996) 397.

[3] H. Dombrowski et al., *Nucl. Instr. & Meth.* **A 386** (1997) 228.

[4] G. Anton et al., *Nucl. Instr. & Meth.* **A 310** (1991) 631.

[5] D. Albers et al., *Phys. Rev. Lett.* **78** (1997) 1652.

[6] F. Lenz, *Nucl. Phys.* **B 279** (1987) 119.

[7] P. Moskal et al., *Phys. Rev. Lett.* **80** (1998) 3202.

[8] H.O. Meyer et al., *Phys. Rev. Lett.* **65** (1990) 2846, H.O. Meyer et al., *Nucl. Phys.* **A 539** (1992) 633, A. Bondar et al., *Phys. Lett.* **B 356** (1995) 8, A.M. Bergdolt et al., *Phys. Rev.* **D 48** (1993) 2969, E. Chiavassa et al., *Phys. Lett.* **B 322** (1994) 270, H. Calén et al., *Phys. Lett.* **B 366** (1996) 39, F. Hibou et al., *Phys. Lett.* **B 438** (1998) 41.

[9] N. Nikolaev, *COSY News* **3** (1998) 4.

[10] P. Moskal et al., STORI99, 4th Int. Conf. on Physics at Storage Rings, Bloomington, Indiana (USA), Sep 12–16, 1999, *AIP Conference Proceedings*, to be published.

[11] J. Balewski et al., *Phys. Lett.* **B 388** (1996) 859 and *Phys. Lett.* **B 420** (1998) 211.

[12] S. Sewerin et al., *Phys. Rev. Lett.* **83** (1999) 682.

[13] K. M. Watson, *Phys. Rev.* **88** (1952) 1163.

[14] G. Fäldt, C. Wilkin, *Z. Phys.* **A 357** (1997) 241.

[15] V. Flaminio et al., Compilation of cross sections, *CERN–HERA rep.* **79-03** (1979).

[16] A. Gasparian et al., e–Print Archive nucl–th/9909017.

[17] N. Kaiser, *Eur. Phys. J.* **A 5** (1999) 105.

[18] A. Sibirtsev et al., *Nucl. Phys.* **A 646** (1999) 427.

[19] H. Calén et al., *Phys. Lett.* **B 458** (1999) 190.